INL/CON-11-22242
PREPRINT

Testing and Performance Analysis of NASA 5 cm by 5 cm Bi-Supported Solid Oxide Electrolysis Cells Operated in Both Fuel Cell and Steam Electrolysis Modes

IMECE 2011

R. C. O'Brien
J. E. O'Brien
C. M. Stoots
X. Zhang
S. C. Farmer
T. L. Cable
J. A. Setlock

The INL is a
U.S. Department of Energy
National Laboratory
operated by
Battelle Energy Alliance

November 2011

Proceedings of the ASME 2011 International Mechanical Engineering Congress & Exposition
IMECE2011
November 11-17, 2011, Denver, Colorado, USA

IMECE2011-62585

TESTING AND PERFORMANCE ANALYSIS OF NASA 5 CM BY 5 CM BI-SUPPORTED SOLID OXIDE ELECTROLYSIS CELLS OPERATED IN BOTH FUEL CELL AND STEAM ELECTROLYSIS MODES

R.C. O'Brien
Center for Space Nuclear Research / INL
Idaho Falls, Idaho, USA

J.E. O'Brien
Idaho National Laboratory
Idaho Falls, Idaho, USA

C.M. Stoots
Idaho National Laboratory
Idaho Falls, Idaho, USA

X. Zhang
Idaho National Laboratory
Idaho Falls, Idaho, USA

S.C. Farmer
NASA Glenn Research Center
Cleveland, Ohio, USA

T.L. Cable
Praxair
Tonawanda, New York, USA

J.A. Setlock
University of Toledo
Toledo, Ohio, USA

ABSTRACT

A series of 5 cm by 5 cm bi-supported Solid Oxide Electrolysis Cells (SOEC) were produced by NASA for the Idaho National Laboratory (INL) and tested under the INL High Temperature Steam Electrolysis program. The results from the experimental demonstration of cell operation for both hydrogen production and operation as fuel cells is presented. An overview of the cell technology, test apparatus and performance analysis is also provided.

INTRODUCTION AND OVERVIEW OF THE NASA SOEC CELL TECHNOLOGY

There is a growing interest in the development of large-scale non-fossil hydrogen production technologies. This interest is driven by the near-term demand for hydrogen for refining of increasingly low-quality petroleum resources, the expected intermediate-term demand for carbon-neutral synthetic fuels, and the potential long-term demand for hydrogen as an environmentally benign direct transportation fuel [*1-3*]. Additional important non-transportation markets for large-scale hydrogen production include ammonia production and (potentially) carbon-free steel production [*4*]. At present, hydrogen production in North America is based almost exclusively on steam reforming of methane. From a long-term perspective, methane reforming may not be sustainable for large-scale hydrogen production since natural gas is a non-renewable resource that exhibits large volatility in price and since methane reforming and other fossil-fuel conversion processes emit large quantities of greenhouse gases to the environment [*5*]. Non-fossil carbon-free options for hydrogen production include conventional water electrolysis coupled to either renewable (e.g., wind) energy sources or nuclear energy. The renewable-hydrogen option may be viable as a supplementary source, but would be very expensive as a large-scale stand-alone option [*6, 7*]. Conventional low temperature electrolysis coupled to nuclear base-load power can approach economical viability when combined with off-peak power, but the capital cost is high [*8*]. To achieve higher overall hydrogen

production efficiencies, high-temperature thermo-chemical [*9*] or electrolytic processes [*10*] can be used. The required high temperature process heat can be based on concentrated solar energy [*11*] or on nuclear energy from advanced high-temperature reactors [*12*]. From 2003 – 2009, development and demonstration of advanced nuclear hydrogen technologies were supported by the US Department of Energy under the Nuclear Hydrogen Initiative (NHI) [*13*]. High temperature steam electrolysis (HTE) was demonstrated as a feasible technology under this program, which included a 15 kW HTE technology demonstration, achieving a hydrogen production rate in excess of 5000 NL/hr [*14*]. During 2009, the NHI program sponsored a technology down-selection activity by which an independent review team recommended HTE as the most appropriate advanced nuclear hydrogen production technology for near-term deployment [*15*]. HTE research is currently supported by the DOE Office of Nuclear Energy under the Next Generation Nuclear Plant (NGNP) Program.

The ultimate cost of hydrogen production by any technology is dependent on both capital and operating costs. In order to achieve competitive capital costs, HTE cells and stacks must exhibit both high performance and low degradation rates. Although HTE has been successfully demonstrated, our experience to date has indicated that SOEC cell and stack degradation must be improved prior to deployment of HTE as a viable cost-competitive technology. Consequently, the current focus of our research is to identify the mechanisms responsible for accelerated degradation in the electrolysis mode. Once these mechanisms are fully understood and ranked in terms of importance, effective mitigation strategies can be developed. Possible degradation mechanisms include transport of impurities leading to electrode poisoning and deactivation [*16*], coarsening of electrodes [*17*], loss of electrolyte ionic conductivity [*18*], depletion of oxygen vacancies in mixed conducting electrodes [*19, 20*], and electrode delamination [*21*].

Under contract to NASA, Boeing Phantom Works conducted a system study to compare flight performance capabilities of a solid oxide fuel cell (SOFC), a proton exchange membrane fuel cell (PEM), and an internal combustion engine (ICE) system for a 14-day HALE (High Altitude Long Endurance) aircraft [*22*]. The study results indicated SOFC provided significantly longer flight endurance due to its higher efficiency, but that SOFC also required the greatest technology development. The study identified unique technical challenges for the HALE application showing especial importance to reduced stack weight (1 kW/kg target). Commercial fuel cells for land-based applications were ~0.2 kW/kg at the time of this study (2005). To meet NASA's demands for high power to weight SOFC, the ceramics branch at NASA Glenn Research Center is working to prototype an alternative light weight, low volume planar SOFC for aerospace applications. Based on their SOFC technology, NASA has been developing single cells and stacks that are suited to operation in the electrolysis mode of operation for high temperature steam electrolysis. The focus of the NASA research is to develop material sets that lead to cells that exhibit low degradation rates and good efficiencies (low Area Specific Resistances). Under the U.S. Department of Energy (DOE) Next Generation Nuclear Plant (NGNP) program, Idaho National Laboratory (INL) provided funding for the development of the first generation 3-cell stacks and component 5 cm by 5 cm single cells for the evaluation of their hydrogen production efficiencies and degradation rates.

The NASA cells are fabricated by casting and laminating green ceramic tapes. The electrolyte is made by doctor blade casting a solvent-based 8 molar percent yttria stabilized zirconia (8YSZ) ceramic slip to produce electrolyte tapes. The electrode skeletons or scaffolds are aqueous-based and produced by doctor blade casting on a chilled bed (<-20 °C). Micron-size ice crystals from on the Mylar tape that is in contact with the chilled bed and coarsen as they grow outward. Conditions are controlled to maximize in-plane texture. The frozen ceramic tape is placed in a freeze-dryer and the water is sublimated which results in a gradient porous structure of interconnected micro-channels. Macro-channels are subsequently cut into the green tapes using a laser in order to create gas flow channels. To produce cells, tapes are cut to size and laminated. Two freeze-case electrode skeletons are laminated with an electrolyte tape, placing the small pore sides against the electrolyte tape (see Figure 1). The laminated structures are sintered at a temperature of approximately 1450 °C. After sintering, the laminated structures are infiltrated with active electrode materials that are typically composed of metal salts. For the cells tested in this paper, the anodes were infiltrated with nickel nitrate and the cathodes were infiltrated with a combination of nitrates to produce a cobalt-doped lanthanum strontium ferrite (LSCF). A final infiltration of the anodes and cathodes with samarium-doped ceria was also performed for stability enhancement.

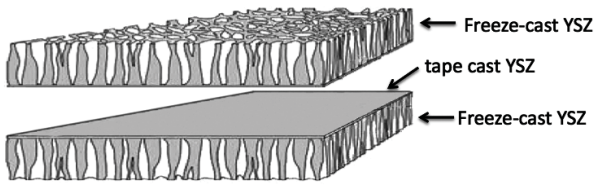

Figure 1: Layup for lamination of the freeze cast electrode skeleton and tape cast electrolyte materials prior to sintering of the SOEC cell structure.

During testing of single cells in electrolysis and in regenerative (reversible) modes of operation at NASA Glenn, the single cells of this design exhibited verify high electrochemical voltage efficiencies (EVE) and high H_2O conversion percentages. An overview of preliminary single cell testing activities and results obtained at INL is presented within this paper.

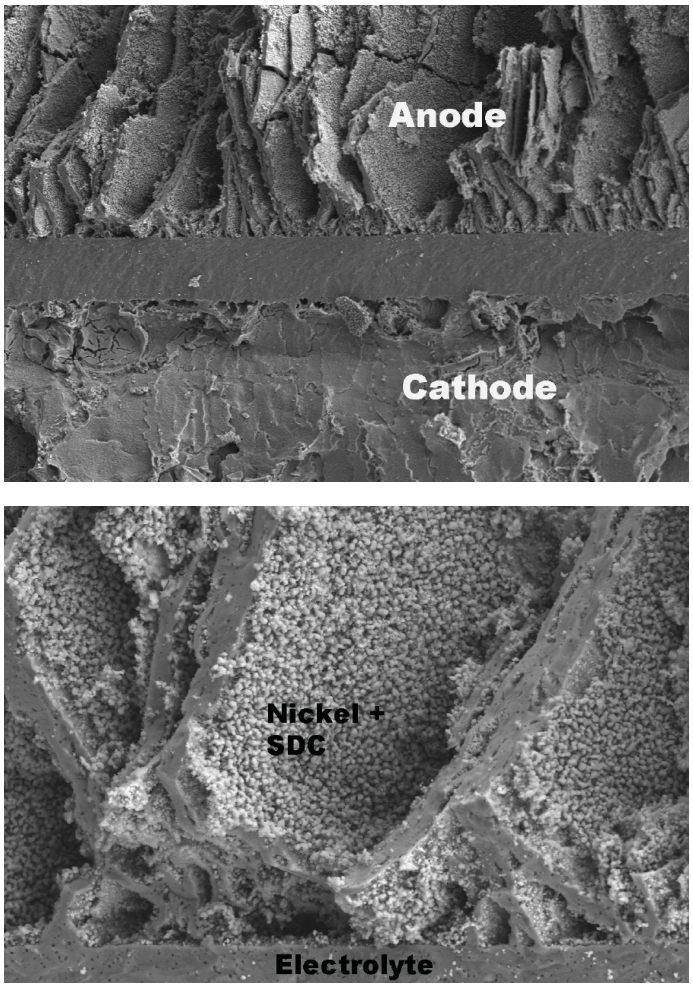

Figure 2: *(Top)* Scanning Electron Microscope (SEM) image of a single SOEC cell cross section. Here, the central band is the 8YSZ electrolyte. Gas flow channels are visible in the anode. (Bottom) High magnification SEM image of anode surface exhibiting polycrystalline structure of nickel and samarium-doped ceria (SDC) infiltration.

NOMENCLATURE

ASR	=	Area-Specific Resistance, Ohm·cm^2
DOE	=	U.S. Department of Energy
EVE	=	Electrochemical Voltage Efficiencies
HTE	=	High Temperature Electrolysis
INL	=	Idaho National Laboratory
NASA	=	National Aeronautics and Space Administration
NGNP	=	Next Generation Nuclear Plant
NHE	=	Nuclear Hydrogen Initiative
SDC	=	Samarium-Doped Ceria
SOEC	=	Solid Oxide Electrolysis Cell
SOFC	=	Solid Oxide Fuel Cell
YSZ	=	Yttria-Stabilized Zirconia

TEST APARATUS

The test aparatus used to test the NASA solid oxide electrolysis cells at Idaho National Laboratory (INL) was initially developed to test Anode-supported Solid Oxide Cells. The original cells tested had a footprint of exactly 5 cm by 5 cm [*23*], thus in order to minimize modifications to the test fixture used to support and seal the cells, an identical cell footprint was adapted for the NASA SOEC single cells.

As illustrated in Figures 3 and 4, a steam hydrogen mixture is supplied to the cell through a ¼ inch inconel coiled tube into the inlet hole in the bottom of the Hastelloy-X (HastX) base plate. It then flows through a diverging flow channel milled into the HastX base plate and passes through a slot in the bottom of the alumina cell holder. The slots can be seen in Fig 2. An alumina felt gasket is used to seal the HastX base plate against the alumina cell holder. The flow then passes under the cell through a corrugated/perforated nickel flow field. The flow field establishes the gap for the steam/hydrogen flow channel under the cell while also serving as an electrical conductor. A 0.254 mm (0.010 in) nickel foil underneath the flow field serves as a current collector. The Ni foil, flow field and mesh are sized to fit into the inner square recess machined into the alumina cell holder. Alumina was selected as the cell holder and air flow distributor material in order to minimize the potential for chromium poisoning of the cell electrodes. The cell holder was machined in the bisque state and then fired. During firing the bisque alumina shrinks by about 15%. This shrinkage must be taken into account when doing the machining such that the desired dimensions are achieved in the final dense alumina part.

A nickel plate welded to a solid inconel bus bar serves as the steam/hydrogen-side cell power supply / current collector. A separate wire is spot welded to the underside of the nickel plate in order to facilitate cell operational voltage measurements. The bus bar and voltage tap wire are insulated with alumina tubes and passed through a central hole in the bottom of the alumina cell holder, and in turn out of the furnace hot-zone.

After passing along the bottom of the cell, the steam/hydrogen flow exits the alumina cell holder through a second slot, flows through a converging passage in the HastX base plate, and out through an 3/8-in OD inconel outlet tube. The outlet tube is sized larger than the inlet tube in order to minimize back pressure on the cell seals to prevent leakage. The cell is placed on a recessed shelf milled into the alumina cell holder just above but in contact with the Ni mesh (see Figure 3). A nickel paste was used to enhance electrical contact between the nickel mesh and flow field foil. An alumina felt gasket is placed on the shelf underneath the cell to help with sealing. In addition, for sealing, an alumina-based ceramic paste (Aremco Products, Ceramabond 552) is distributed around the top outer edge of

the cell to seal the gap between the cell and the alumina cell holder.

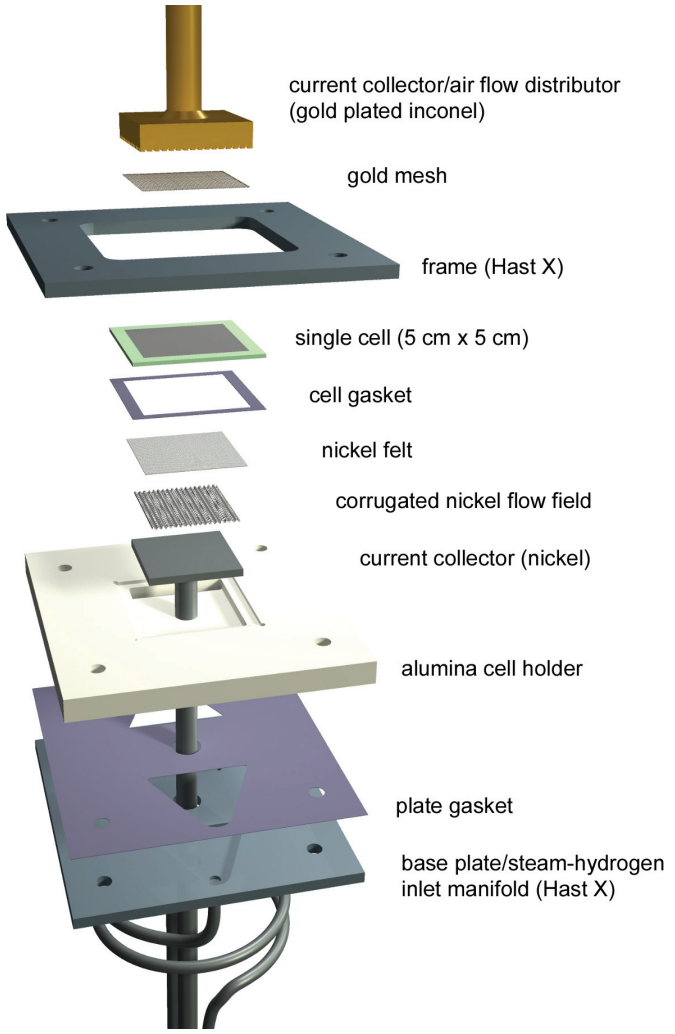

Figure 3: Exploded view of the INL test fixture used to support and seal the NASA 5 cm by 5 cm Solid Oxide Cells while providing steam flow & sweep gas flows.

On the air-side of the cell, a gold mesh is placed in contact with the air-side electrode. This gold mesh is held against the air-side electrode by a gold plated current collector / air flow distributor fabricated from inconel plate. Air is introduced to the top side of the cell through a gold plated inconel inlet tube welded to the current collector / air flow distributor plate. The air inlet tube is double walled in order to serve its second purpose, which is the conduction of electrical current to/from the SOEC air-side electrode. The airflow distributor has an array of square protuberances milled into its surface (see Figure X), creating a gap for airflow while also compressing the gold mesh against the air-side electrode. Several air outlet holes are distributed in the center of airflow distributor. After exiting the airflow distributor, the air impinges on the cathode side of the cell and flows radially outward through the array of protuberances. After sweeping the air-side electrode, the air exits into the furnace volume. An airside electrode voltage tap wire, insulated by alumina tubing and beads, is spot welded to the airflow distributor and runs alongside the air inlet tube/current collector and out of the furnace hot-zone for connection to the test stand data acquisition system.

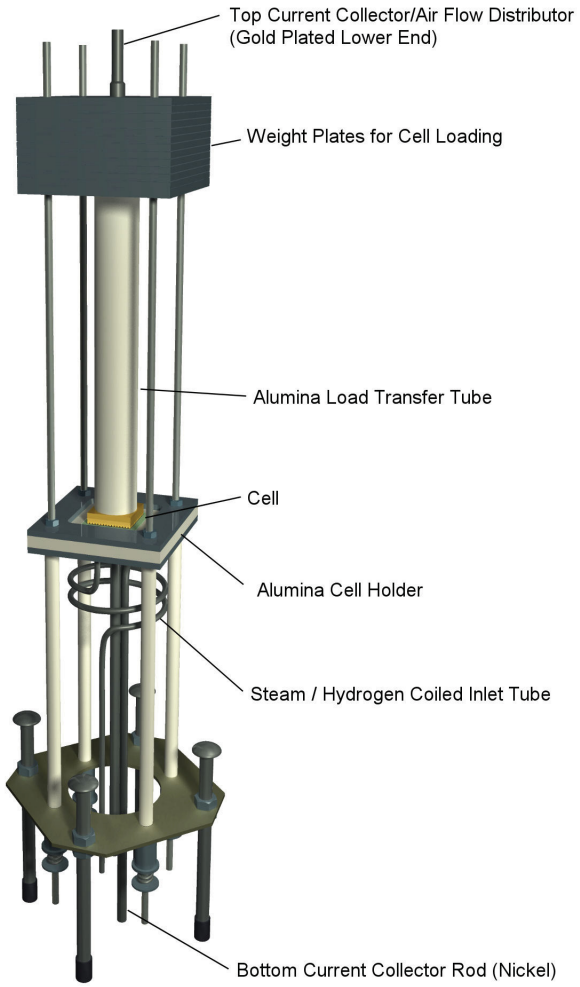

Figure 4: Overview of the 5 cm by 5 cm cell test fixture and hot-zone apparatus.

A fixed compressive load is applied to the entire cell stack up between the alumina cell holder and an alumina load tube/inconel pusher plate by means of weights, as shown in Figure 2. This load simultaneously compresses the cell against the nickel mesh, flow field and foil on the bottom steam/hydrogen side of the cell and against the gold mesh on the air side. It also compresses the cell against the seal around the outer edge of the cell which rests on the shelf milled into the alumina cell holder. The HastX weight plates are held in alignment by the upper portion of threaded rods which extend upward from the base of the test fixture for this purpose. A fixed compressive load is independently applied between the

HastX frame, the alumina cell holder, and the HastX base plate. This load is generated by the compression of four springs located under the test stand base support outside of the furnace. The springs are compressed a fixed amount that is determined by the height of underside spool pieces and by the tightening of a nut on the threaded rods. The threaded rods are fed through the alumina spacer tubes. These spacer tubes determine the height of the cell holder inside the furnace. The spring-generated load is intended to compress the seal between the cell holder and the base plate. This seal was formed by alumina felt impregnated with alumina slurry. A nut is visible on the threaded rods in Fig. 4 just above the HastX frame and below the weight plates. This nut represents the upper stop for this compressive load. The extension of the threaded rods above the nuts is for the purpose of aligning the weight plates. Note that the weight plates are floating above these nuts since they are resting on the HastX top plate.

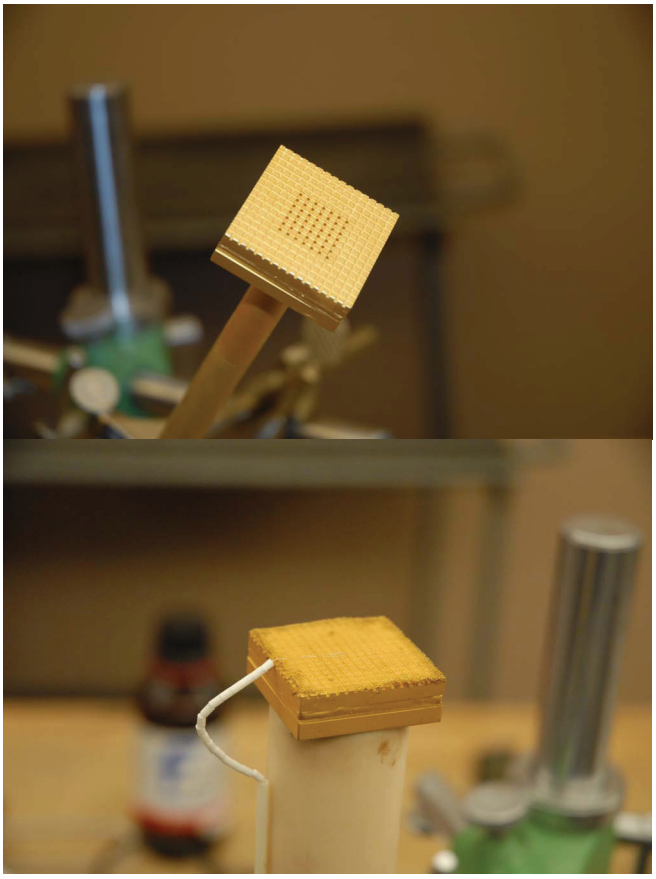

Figure 5: *(Top)* Photograph of the underside of the gold plated airflow distributor / current collector. Here, the square milled protuberances and air outlet holes are visible. *(Bottom)* Photograph of the current collector / airflow distributor assembly prior to installation atop of an SOEC. Here the gold mesh and insulated voltage tap wire are visible.

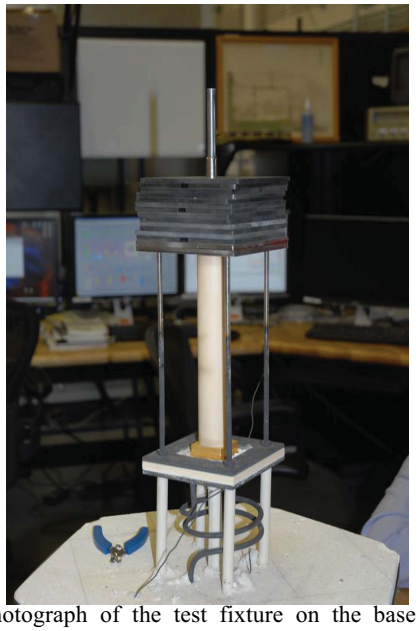

Figure 6: Photograph of the test fixture on the base plate of the furnace. Note that the base support outlined at the bottom of Figure 2 is located outside of the furnace hot-zone.

A photograph of the test stand installed in the furnace base is provided in Figure 6. Note that the base support is located outside of the furnace hot-zone. Holes were drilled in the bottom of the furnace for pass-through of the flow tubes, the alumina spacer rods, power leads and instrumentation.

A process flow diagram for the experimental apparatus used for single-cell testing is presented in Figure 7. Primary components include gas supply cylinders, mass-flow controllers, a heated water-bath humidifier, on-line dew point sensors, temperature and pressure measurement, high temperature furnace, and the solid oxide electrolysis cell. Nitrogen is used as an inert carrier gas. Inlet flow rates of nitrogen, hydrogen, and air are established by means of precision mass-flow controllers. Hydrogen is included in the inlet flow as a reducing gas in order to prevent oxidation of the nickel cermet electrode material. Air flow to the cell is supplied by the shop air system, after passing through a two-stage extractor / dryer unit. The cathode-side inlet gas mixture, consisting of hydrogen and nitrogen is mixed with steam by means of a heated humidifier. The dew point temperature of the nitrogen / hydrogen / steam gas mixture exiting the humidifier is monitored continuously using a precision dew point sensor. All gas lines located downstream of the humidifier are heat-traced in order to prevent steam condensation. Prior to the exhaust of process gases from the test apparatus, the gas stream is cooled via a bubbler condenser. The cooled exhaust product of hydrogen and nitrogen is vented to a stack on the facility roof however, the product stream may optionally be compressed and stored for further experimentation such as reversed operation in SOFC mode through reaction of SOEC products.

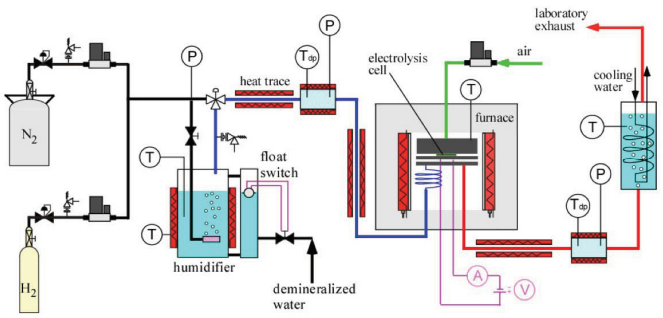

Figure 7: Process flow diagram for the single cell test apparatus.

Real time test data is collected from in-line instrumentation within a National Instruments Labview™ based virtual interface (VI) through an Agilent data acquisition unit. Control of the test aparatus temperature and process fluid controls is provided via a Measurement Computing™ USB DAC interface coupled to solid-state relays and mass flow controllers respectively. A lambda™ power supply is used to provide electrical power to a stack while operated in the steam electrolysis mode. An Amrel electronic load is used as a power sink for operation of cells in the fuel cell mode. Switching between the power supply and the electronic load is facilitated by a network of electronic relays housed within a switching box. Both the electronic load and power supply is controlled through the National Instruments Labview™ VI allowing for data acquisition and control of DC-potential sweeps for cell performance characterization.

TEST PROCEDURE

The single cells as supplied by NASA are previously reduced, thus heat-up and start-up of cell testing was simplified. The cells tested in this study were operated at a temperature of 850 °C for long-term testing in the electrolysis mode. Several stages of heat-up and staged cell characterization were performed. Table 1 summarizes the test conditions adopted. The heat-up profile for the furnace had a ramp rate of 2 °C per minute. A safe forming gas consisting of 95% nitrogen and 5 % hydrogen was provided through the test section during the second stage of heat up (between 450 and 750 °C) to prevent oxidation of the nickel test fixture components and re-oxidation of the cell steam hydrogen electrode. Once at 750 °C, the gas flows were increased to allow for initial characterization of cell performance in the SOFC mode of operation (See Table 1). This initial characterization of the cell performance was determined through a DC-potential (V-I) sweep obtained with dry inlet conditions in the fuel cell mode of operation via the use of the Amrel electronic load over the current density range of 0 to 0.5 A/cm^2. The nominal active area for the cells tested throughout this study was 16 cm^2. Having characterized SOFC performance at 750 °C, this procedure was repeated at 800 °C and 850°C. Upon completion of dry SOFC characterization at 850 °C, steam was introduced to the cell via the humidifier for SOFC and SOEC characterization from -0.5A/cm^2 to +0.5A/cm^2 for dew point conditions of 25 °C, 50 °C and 68°C. SOEC potential sweeps were facilitated through the operation of a Lambda GEN20-38 (20V - 30 A) power supply controlled via the Labview virtual interface. The power supply was also used for provision of power during long term SOEC operation.

Step	*Temperature (°C)*	*Dew Point (°C)*	*H_2 Flow (SLPM)*	*N_2 Flow (SLPM)*	*Airside Flow (SLPM)*
1	0 → 450 @ 5 °C/min	0	0	0	0
2	450 → 750 @ 2 °C/min	0	7.5	142.5	150.0
3	750 Hold for SOFC characterization	0	500.0	500.0	1000.0
4	750 Hold for SOFC characterization	0	500.0	500.0	1000.0
5	750 → 800 @ 2 °C/min	0	500.0	500.0	1000.0
6	800 Hold for SOFC characterization	0	500.0	500.0	1000.0
7	800 → 850 @ 2 °C/min	0	500.0	500.0	1000.0
8	850 Hold for SOFC and SOEC characterization	0	500.0	500.0	1000.0
9	850 Hold for SOFC and SOEC characterization	25	500.0	500.0	1000.0
10	850 Hold for SOFC and SOEC characterization	50	500.0	500.0	1000.0
11	850 Hold for SOFC and SOEC characterization	68	500.0	500.0	1000.0
12	850 Long term SOEC operation with mid-term and end SOEC/SOFC mode characterization	68	300	300	1000.0

Table 1: Summary of the NASA single 5 cm by 5 cm single cell heat-up procedure and operating conditions. Step number is referred to by results data in discussion of operating conditions.

After the series of initial cell characterizations were performed, the gas flows were adjusted to provide equal inlet conditions of 33 $\%_{Mol}$ steam, hydrogen and nitrogen for steady state long term testing in the SOEC mode. Once the gas flows and OCV had stabilized, a DC-potential sweep for SOFC and SOEC characterization from -0.5A/cm^2 to +0.5A/cm^2 was repeated before placing the cell into constant current SOEC operation with a current density of 0.5 A/cm^2 and 0.2 A/cm^2 for the first and second cells tested in this study respectively. During cell test 1, the current density was reduced to 0.2 A/cm^2 after 86 hours when the ASR had increased by a factor of 2.62. The lowering of the current density was used to provide an initial

estimate of the relationship between current density and degradation rate.

The two initial cell tests presented within this paper were operated in long term SOEC mode for approximately 95 and 114 hours respectively. Prior to the shutdown of cells held under long-term test, final DC-potential sweeps were performed in both SOFC and SOEC modes of operation.

PRELIMINARY RESULTS

After initial cell characterization was complete at the beginning of each test, the cells were placed into a long-term SOEC mode of operation. Figure 8 below illustrates the Area Specific resistances and cell operating voltages as a function of time for each test. The cell in Test 1 was operated at a current density of 0.5 A/cm^2 for the first 86 hours and lowered to 0.2 A/cm^2. The cell in Test 2 was operated at 0.2 A/cm^2 throughout the test. Mid-term DC-potential sweeps were performed at approximately half way through each test. These appear as vertical lines in data. The DC-potential sweep data acquired during initial cell characterization, mid-term and at the end of each test are plotted on figures 9 and 10 for tests 1 and 2 respectively.

The open cell voltages (OCVs) of the cells at each measurement stage can be determined through the examination of figures 9 and 10 on the respective y-axis intercepts (I = 0 A). Both cells behaved consistently during initial characterization. The Dry OCV values at the peak operating temperature of 850 °C in both cases was approximately 1.03 Volts. Similarly, when steam was introduced to the cells at 33 %$_{Mol}$, both cells had an OCV of 0.911 Volts. The OCV values at the test termination points differed as anticipated due to the cell degradation process, the rate of which was driven by the test conditions.

The initial cell characterizations illustrated through the DC-potential sweeps presented in figures 9 and 10 demonstrate the cells' expected responses to the changes in both operating temperature and steam content. Cell degradation is clearly exhibited in the DC-potential plots and the change in the gradients of each time dependant sweep is directly proportional to the increase in area specific resistance [*23*].

Examination of the cell voltages in Figure 8 can yield estimates for the cell degradation rates. For the cell in test number 1 while operated at a current density of 0.5 A/cm^2, the apparent cell degradation rate was approximately 323 % per thousand hours of operation. When its current density was reduced to 0.2 A/cm^2 during the final 9 hours of test number 1, the cell exhibited an apparent degradation rate of 109 % per thousand hours of operation. The cell operated at 0.2 A/cm^2 throughout test number 2 exhibited an apparent degradation rate of approximately 100 % per thousand hours. Thus, for the single cells tested, there is a clear relationship between current density and cell degradation rates.

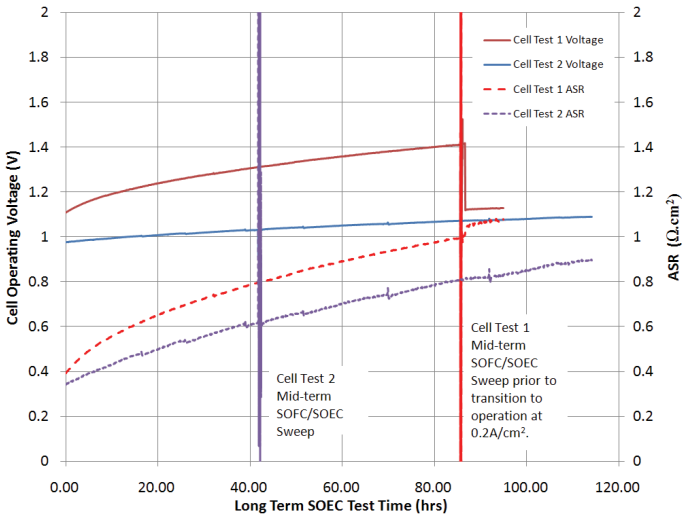

Figure 8: Long term cell voltages and ASR values for Test 1 and Test 2. The cell in Test 1 was operated at a current density of 0.5 A/cm^2 for the first 86 hours and lowered to 0.2 A/cm^2. The cell in Test 2 was operated at 0.2 A/cm^2 throughout the test. Mid-term DC-potential sweeps appear as vertical lines in data.

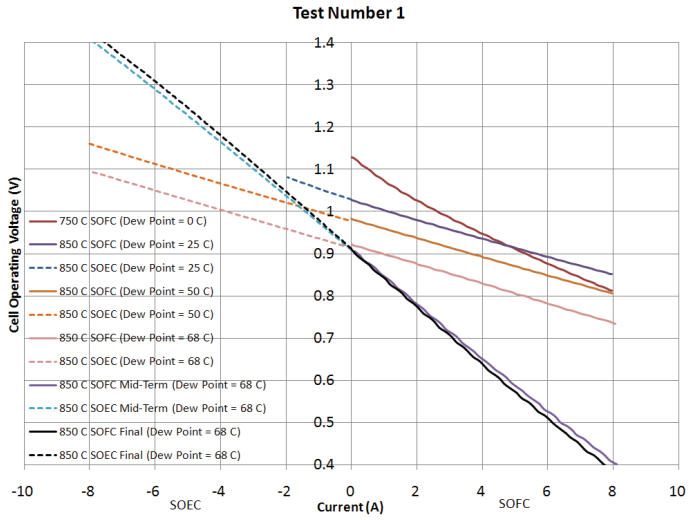

Figure 9: DC-potential sweeps for initial, mid-term and final stages of long term SOEC operation during test number 1. 9 hours separate the mid-term and final sweeps.

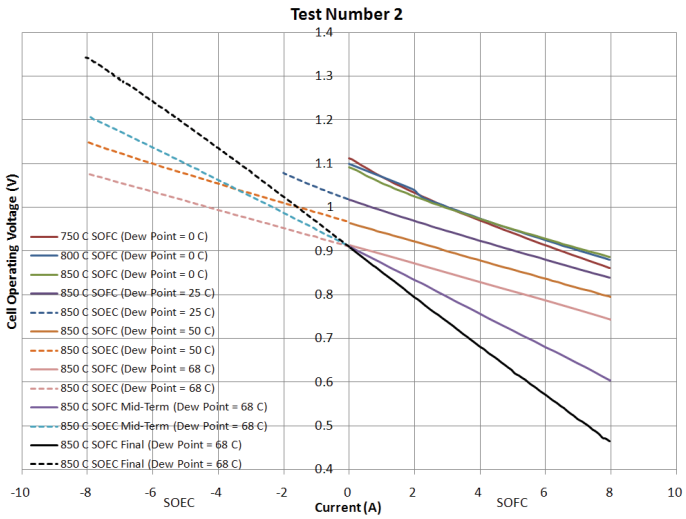

Figure 10: DC-potential sweeps for initial, mid-term and final stages of long term SOEC operation during test number 2. The effect of operating temperature and inlet dew point upon cell performance in the SOFC mode is demonstrated.

SUMMARY AND CONCLUSIONS

The INL High Temperature Steam Electrolysis laboratory has developed significant test infrastructure in support of single cell and stack performance analyses. An overview of the single cell test apparatus is presented.

The test data presented in this paper is representative of a first batch of NASA's prototypic 5 cm by 5 cm SOEC single cells. Clearly a significant relationship between the operational current density and cell degradation rate is evident. While the performance of these cells was lower than anticipated, in-house testing at NASA Glenn has yielded significantly higher performance and lower degradation rates with subsequent production batches of cells. Current post-test microstructure analyses of the cells tested at INL will be published in a future paper.

Modification to cell compositions and cell reduction techniques will be altered in the next series of cells to be delivered to INL with the aim to decrease the cell degradation rate while allowing for higher operational current densities to be sustained. Results from the testing of new batches of single cells will be presented in a future paper.

ACKNOWLEDGMENTS

The authors of this article wish to thank the United States Department of Energy and the Next Generation Nuclear Plant Program directorate for its sponsorship of this work.

REFERENCES

[1] C.W. Forsberg, "The Hydrogen Economy is Coming. The Question is Where". *Chemical Eng. Progress.* (2005) pp. 20-22.

[2] D. Lewis, "Hydrogen and its relationship with nuclear energy". *Progress in Nuclear Energy.* 50 (2008) 394-401.

[3] P. Kruger, "Nuclear Production of Hydrogen as an Appropriate Technology". *Nuclear Technology.* 166 (2009) 11-17.

[4] C.W. Forsberg, "Future hydrogen markets for large-scale hydrogen production systems". *Int. J. Hydrogen Energy.* 32 (2007) 431-439.

[5] R.B. Duffey, "Nuclear production of hydrogen: When worlds collide". *International Journal of Energy Research.* 33 (2009) 126-134.

[6] M. Granovskii, I. Dincer, M.A. Rosen, "Greenhouse gas emissions reduction by use of wind and solar energies for hydrogen and electricity production: economic factors". *Int. J. Hydrogen Energy.* 32 (2007) 927-931.

[7] D.A.J. Rand, R.M. Dell, "Hydrogen Energy: Challenges and Prospects". *Royal Society of Chemistry.* (2008).

[8] P-H Floch, S. Gabriel, C. Mansilla, F. Werkoff, "On the production of hydrogen via alkaline electrolysis during off-peak periods". *Int. J. Hydrogen Energy.* 32 (2007) 4641-4647.

[9] K.R. Schultz, L.C. Brown, G.E. Besenbruch, C.J. Hamilton, "Large-Scale Production of Hydrogen by Nuclear Energy for the Hydrogen Economy". *Report GA-A24265.* (2003).

[10] J.E. O'Brien, C.M. Stoots, J.S. Herring, J.J. Hartvigsen, "Performance of Planar High-Temperature Electrolysis Stacks for Hydrogen Production from Nuclear Energy". *Nuclear Technology.* 158 (2007) 118-131.

[11] A. Steinfeld, "Solar thermochemical production of hydrogen". *Solar Energy.* 78 (2005) 603-615.

[12] F. Southworth, P.E. MacDonarl, D.J. Harrell, et al. "The Next Generation Nuclear Plant (NGNP) Project". *Global 2003*; 2003: pp. 276-287.

[13] K. Schultz, C. Sink, P. Pickard, et al., "Status of the US Nuclear Hydrogen Initiative". *Societe Francaise d'Energie Nucleaire.* ICAPP (2007) 2932-2940.

[14] C.M. Stoots, J.E. O'Brien, K. Condie, et al., "The High-Temperature Electrolysis Integrated Laboratory Experiment". *Nuclear Technology.* April (2009).

[15] R.D. Varrin, K. Reifsneider, D.S. Scott, P. Irving, G. Rolfsen, "NGNP Hydrogen Technology Down-Selection; Results of the Independent Review Team Evaluation". *Dominion Engineering report R-6917-00-01.* (2009).

[16] A. Hauch, "Solid Oxide Electrolysis Cells – Performance and Durability". *PhD Thesis, Technical University of Denmark, Risø National Laboratory, Roskilde, Denmark.* (2007).

[17] P. Tanasini, M. Cannarozzo, P. Costamagna, et al., "Experimental and theoretical investigation of degradation mechanisms by particle coarsening in sofc electrodes". *Fuel Cells.* 9 (2009) 740-752.

[18] B. Butz, P. Kruse, H. Stormer, et al., "Correlation between Microstructure and Degradation in Conductivity for Cubic Y2O3-doped ZrO2". *Solid State Ionics.* 177 (2006) 3275-3284.

[19] O.A. Marina, L.R. Pederson, M.C. Williams, et al., "Electrode Performance in Reversible Solid Oxide Fuel Cells". *J. Electrochemical Soc.* 154 (2007) B452-B459.

[20] A.M. Svensson, S. Sunde, K. Nisancioglu, "Mathematical Modeling of Oxygen Exchange and Transport in Air-Perovskite-Yttria-Stabilized Zirconia Interface Regions". *J. Electrochemical Soc.* 145 (1998) 1390-1400.

[21] A.V. Virkar, "Mechanism of Oxygen Electrode Delamination in Solid Oxide Electrolyzer Cells". *Int. J. Hydrogen Energy, in review.* (2010).

[22] C.L. Nickol, M.D. Guynn, L.L. Kohout, T.A. Ozoroski. "*High Altitude Long Endurance UAV Analysis of alternatives and Technology Requirements Development".* Langley Research Center, Hampton, VA. NASA/TP-2007-214861. (2007).

[23] J.E. O'Brien, G.K. Housley, D.G. Milobar, N. Petigny. "Performance of single electrode-supported cells operating in the electrolysis mode". *The 2009 International Mechanical Engineering Congress and Exposition (IMECE2009)*. Lake Buena Vista, FL: ASME; 2009.